Solid State Science and Technology, Vol. 31, No 1 (2023), 1-10
ISSN 0128-7389 | *http://myjms.mohe.gov.my/index.php/masshp*

EFFECT OF NICKEL OXIDE DOPING CONCENTRATION ON STRUCTURAL AND MORPHOLOGICAL PROPERTIES OF ZINC OXIDE PREPARED BY PRECIPITATION METHOD

Syazni Hanun Nur Ili Dedy Dasiano[1], Kamil Muhammad Yusoff[1], Mohamad Hafiz Mamat[2], Muhd Firdaus Kasim[3], Hartini Ahmad Rafaie[4,*]

[1]*Faculty of Applied Sciences, Universiti Teknologi MARA, 40450 Shah Alam Selangor, Malaysia*

[2]*NANO-Electronic Centre, Faculty of Electrical Engineering, Universiti Teknologi MARA, 40450 Shah Alam Selangor, Malaysia*

[3]*Centre for Nanomaterials Research, Institute of Science, Universiti Teknologi MARA, 40450 Shah Alam Selangor, Malaysia*

[4]*Centre of Foundation Studies, Universiti Teknologi MARA, Selangor Branch, Dengkil Campus, 43800 Dengkil, Selangor, Malaysia*

**Corresponding author e-mail: hartinirafaie@uitm.edu.my*

Received: 1 August 2022; Accepted: 25 August 2022

ABSTRACT

Zinc oxide (ZnO) is one of the most important II-VI semiconducting materials with wide band gap, whose nanostructures and nanoparticles have attracted the attention and research efforts of many material scientists due to its broad range of applications. This study aimed to examine how nickel oxide (NiO) content affects the structural and morphological properties of the ZnO. Undoped ZnO and NiO-doped ZnO were synthesized using precipitation method at various mol % concentration of NiO. The synthesized NiO-doped ZnO was characterized by the following techniques: Powdered X-ray diffraction analysis (PXRD), Scanning Electron Microscope (SEM) with Energy Dispersive X-ray Analysis (EDX) and Fourier transformed infra-red spectroscopy (FTIR), respectively to investigate the phase structure, morphological structure together with elemental existence and chemical bond of the prepared samples. XRD patterns revealed that ZnO particles have a hexagonal wurtzite structure and NiO particles have a cubic structure with the estimated crystallite size of 40.6 – 47.6 nm. The Ni ion was successfully incorporated into the Zn lattice, confirmed by (101) peak shifting from the XRD results. The microscopy image exhibits the presence of thin nanoflake structures. The results indicated that the nanoflakes structures agglomerate and become more prominent as molar concentration increases. The elemental compositions of Zn, Ni, and O are confirmed by EDX analysis. The various mol % concentration of NiO to ZnO was found significantly affected the phase structure and morphological properties of the

obtained sample. Overall, this work is of great significance for understanding the effect of doping concentration towards promising areas of application such as photocatalysis, gas sensors and solar cells.

Keywords: Doping; NiO; Precipitation; ZnO

INTRODUCTION

In recent years, most researchers in materials sciences have been focusing on semiconductor material with wide a band gap. One of tremendous semiconductor material is zinc oxide (ZnO), which exhibit multifunctionalities due to its magnificent properties and applicability in various applications. On top of its excitonic binding energy (60 meV) and significant energy gap (3.37 eV) [1], ZnO has capabilities in several fields, which would include photocatalysis [2], gas sensing devices [3], and solar cells [4] owes to notably strong DC electrical conductivity and excellent visible transparency spectrum. Moreover, the advantages of ZnO micro and nanostructures include abundance, low cost and non-toxicity material [5]. Therefore, ZnO is considered as a promising functional material due to its electrical, optoelectronic and luminescent properties. Doping with transition metals was recently highly explored and researched to create an improved and excellent ZnO nanostructures [6]. Nickel oxide (NiO) is a p-type transparent, broad direct band gap 3.6–4.0 eV semiconductor with important electronics, chemical, magnetic, and electrical characteristics [1]. Research has consistently demonstrated that doping NiO into a ZnO matrix improves the material's characteristics and effectiveness as NiO concentration rises [7-9].

Diverse fabrication methods have been utilized to create ZnO nanostructures, including sol-gel deposition [10], a chemical co-precipitation method [11], a hydrothermal [12], and a thermal decomposition method [13]. Different techniques result in different properties of the ZnO nanostructures. According to previous studies, vapour phase growth techniques such as molecular beam epitaxy (MBE) [14], metal–organic chemical vapour deposition (MOCVD) [15][16], and sputtering deposition [17][18] were generally used to create ZnO nanostructures. However, the expenses of these procedures are high due to the complicated equipment setup, and they are not cost effective in terms of manufacturing. Precipitation technique is a reasonably simple and straightforward procedure that operates at a lower temperature [19][20]. Nonetheless, several characteristics of the NiO-ZnO nanoparticles remain contentious, necessitating more research to explain this uncertainty and create more excellent uniformity amongst these characteristics. Therefore, in this work, undoped ZnO and NiO doped ZnO was successfully prepared at variation mol % concentration of NiO i.e., 10, 20, 30, 40, and 50 mol % respectively by a simple and inexpensive precipitation method. Overall structural and chemical bonding characteristics of the produced samples were characterized.

METHODS

For the synthesis of undoped ZnO and NiO-doped ZnO, the analytical grade of zinc nitrate hexahydrate [Zn $(NO_3)_2.6H_2O$], nickel nitrate hexahydrate [Ni $(NO_3)_3 \cdot 6H_2O$] and sodium

hydroxide (NaOH) were used. All the reagents used in the present work were of analytical grade and received from Sigma Aldrich without further purification. Synthesis of undoped ZnO and NiO-doped ZnO was done using a simple and inexpensive precipitation method with different mol % concentration of NiO ranging from 10 – 50 mol %. In a typical reaction process, 14.87 g zinc nitrate hexahydrate was dissolved in 500 ml deionized (DI) water and 0.1 M NaOH was added dropwise until the pH solution was 11. NiO-doped ZnO was synthesized with 2.94, 5.88, 8.82, 11,77 and 14.71 g of nickel nitrate were added to the stock solutions, corresponding to 10, 20, 30, 40 and 50 mol % Ni with respect to zinc. The solution was placed on a hot plate, was continuously stirred at 120 °C for 1 h and left for 24 h. The precipitates were extracted from the solution and rinsed three times. The undoped ZnO and NiO-doped ZnO powder obtained was calcined at 300 °C for 2 h on a hot plate. The obtained samples in coarse powders were grounded into finer powders using an agate mortar and pestle. All samples were prepared in the same experimental conditions as represents in Figure 1.

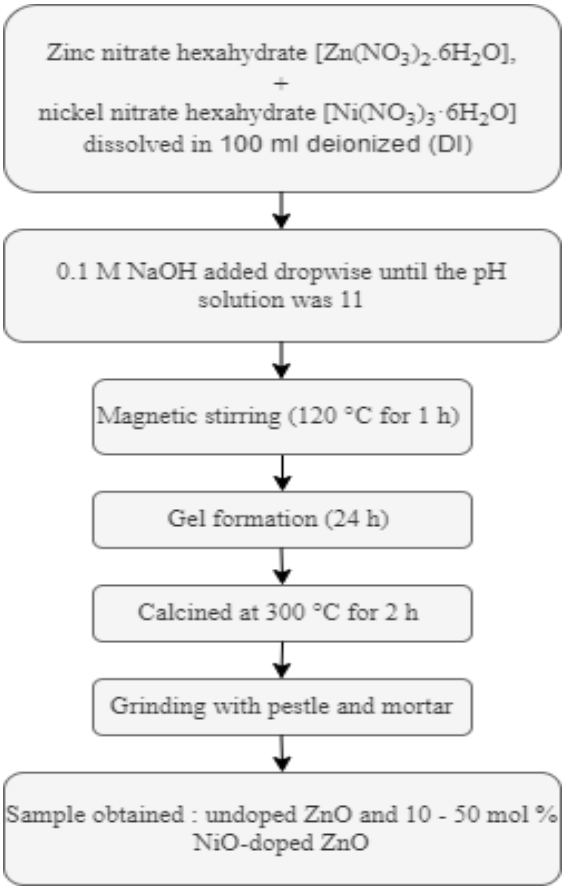

Figure 1: Flowchart for the preparation of undoped ZnO and NiO-doped ZnO by precipitation method

The following instruments were used for the characterization of the prepared samples. The structure and crystallinity of the undoped ZnO and NiO-doped ZnO were

analyzed using XRD (PANalytical X'Pert PRO with Cu Kα radiation, λ=1.54 Å). The diffraction patterns were recorded at Bragg's (2θ) in the range of (30–70°) with a scan rate of 0.02° per minute. Morphological properties of the undoped ZnO and NiO-doped ZnO and their elemental composition were investigated by scanning electron microscope (SEM) operating at 15 kV equipped with energy-dispersive X-ray spectroscopy (SEM-EDS, TESCAN VEGA3). The prepared undoped ZnO and NiO-doped functional groups were analyzed by Perkin Elmer Fourier transform infrared (FT-IR, Spectrum 100) spectrometer between 4000 to 400 cm^{-1} using the attenuated total reflection (ATR) accessory.

RESULTS AND DISCUSSION

The crystalline structure of prepared sample NiO-doped ZnO were obtained and studied by the assist of X-ray diffractometer having Kα radiation of Cu (λ=1.54 Å). Figure 2 represents the XRD spectra of undoped ZnO and NiO-doped ZnO at different mol % of 10, 20, 30, 40 and 50, respectively. The result shows that the XRD pattern of NiO-doped ZnO samples was pure and crystalline. The peaks at 31.70, 34.38, 36.18, 47.46, 56.46, 62.76, 66.22, 67.81, 68.92, 72.47, 76.79, 81.26 and 89.42 can be indexed to (100), (002), (101), (102), (110), (103), (200), (112), (201), (004), (202), (104) and (203) planes and these were consistent with hexagonal wurtzite ZnO (JCPDS 01-079-0207) [3]. However, some additional peaks with weak intensity (designated by asterisk) are observed at 2θ = 38.11º (111) and 2θ = 43.25º (200) and attributed to the secondary phase of the NiO structure, which appeared and grew with an increasing NiO concentration (Figure 2a and b) [1][4]. A slightly peak (101) shifted can be observed as the doping concentration increases as represent in Figure 2 (c). This can be attributed to the smaller ionic radius of the Ni^{2+} ion (0.55 Å) compared to the Zn^{2+} ion (0.60 Å). This finding is consistent with work by Nsib et al. (2016) and Nada et al. (2018) which found that doping causes the wurtzite peaks of ZnO slightly shifted, demonstrating that Ni^{2+} is incorporated into the ZnO lattice [21,22].

The average crystallite size of undoped ZnO and NiO-doped ZnO at various mol % concentrations had been obtained and calculated using Scherrer's equation as in Eq. (1) below [5,23]:

$$D = \frac{k\lambda}{\beta\cos\theta} \tag{1}$$

where average crystallite size is denoted by D, k is the Scherrer constant (k = 0.89), λ represents the incident X-ray wavelength, θ is the Bragg diffraction angle, and β refers to the peak full width at half maximum (FWHM) of the sample. The undoped ZnO and NiO-doped ZnO at different mol % concentrations were in the range of 40.6–47.6 nm, respectively. Table 1 provided the crystallite size data for undoped ZnO and NiO-doped ZnO at a various mol% concentration. The crystallite size of the NiO-doped ZnO had decreased initially from 0 mol % to 30 mol % of NiO, then increased at higher mol % of NiO and possessed a higher value compared to that of the undoped ZnO.

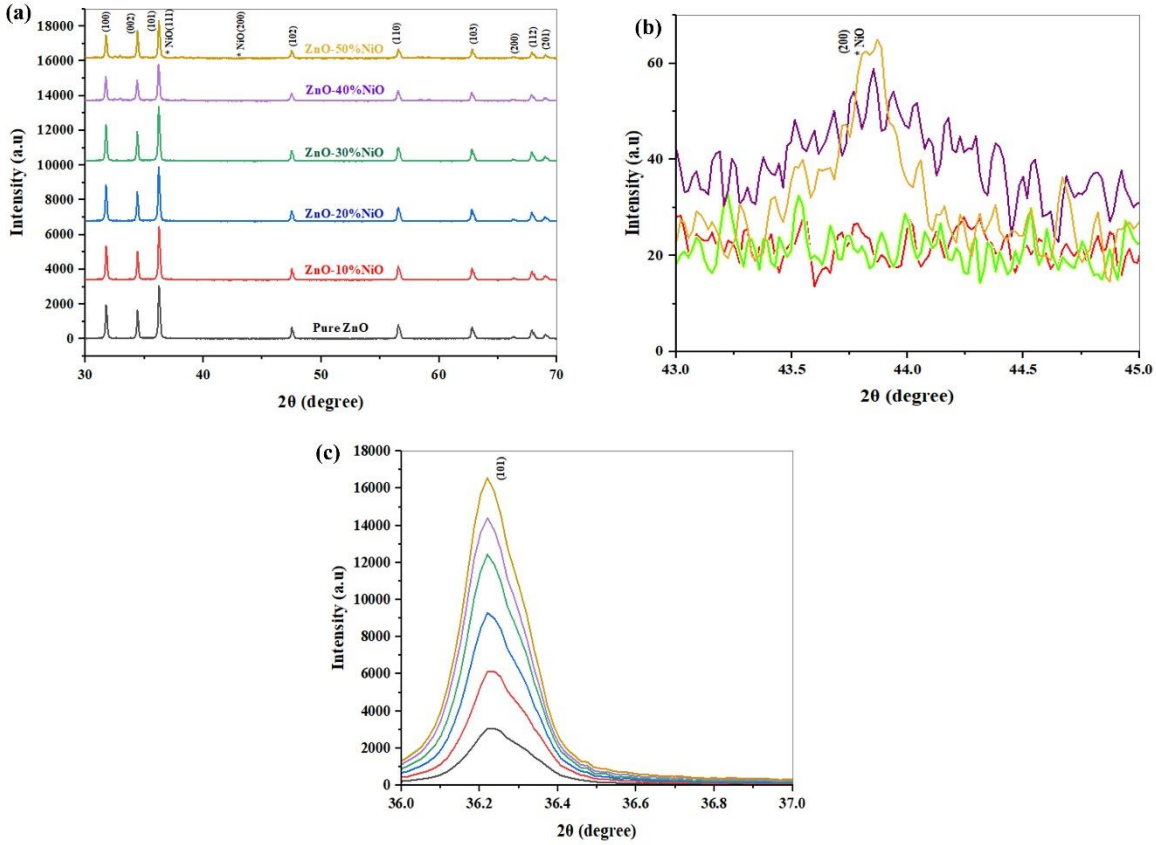

Figure 2: (a) XRD patterns, (b) (200) peaks related to the secondary phase of structure and (c) shift of main peak (101) of pure ZnO and NiO-doped ZnO (10, 20, 30, 40 and 50 mol %)

Table 1: XRD data of NiO-doped ZnO in (101) reflection plane

Sample	2θ (degree)	FWHM, β(degree)	Average crystallite size, D (nm)
Undoped ZnO	36.27	0.18789	44.16
NiO	43.25	0.48356	17.16
ZnO-10%NiO	36.19	0.19126	43.38
ZnO-20%NiO	36.21	0.19403	42.76
ZnO-30%NiO	36.21	0.19276	43.05
ZnO-40%NiO	36.20	0.20439	40.60
ZnO-50%NiO	34.52	0.17436	47.60

The morphological analysis was conducted for undoped ZnO and 10-50 mol% NiO-doped ZnO, as presented in Figure 3. Figure 3 (a) represents the undoped ZnO, (b)–(f) 10-50 mol % NiO-doped ZnO carried out at the same magnification. As depicted in Figure 3 (a) – (f), the undoped ZnO and NiO-doped ZnO samples were mainly consist of flakes-like particles that were evenly distributed and well dispersed with sizes ranging from 100 to 500 nm, respectively. The surface of the flakes-like undoped ZnO, 10 and 20

mol % NiO-doped ZnO having agglomeration which confirms the presence of both particles due to the high surface energy of the particles during synthesis, thus particles tend to reduce the surface energy by agglomeration [22]. Moreover, with the increase of NiO content, the surface of the flake's structures become less agglomerate, and it becomes prominent.

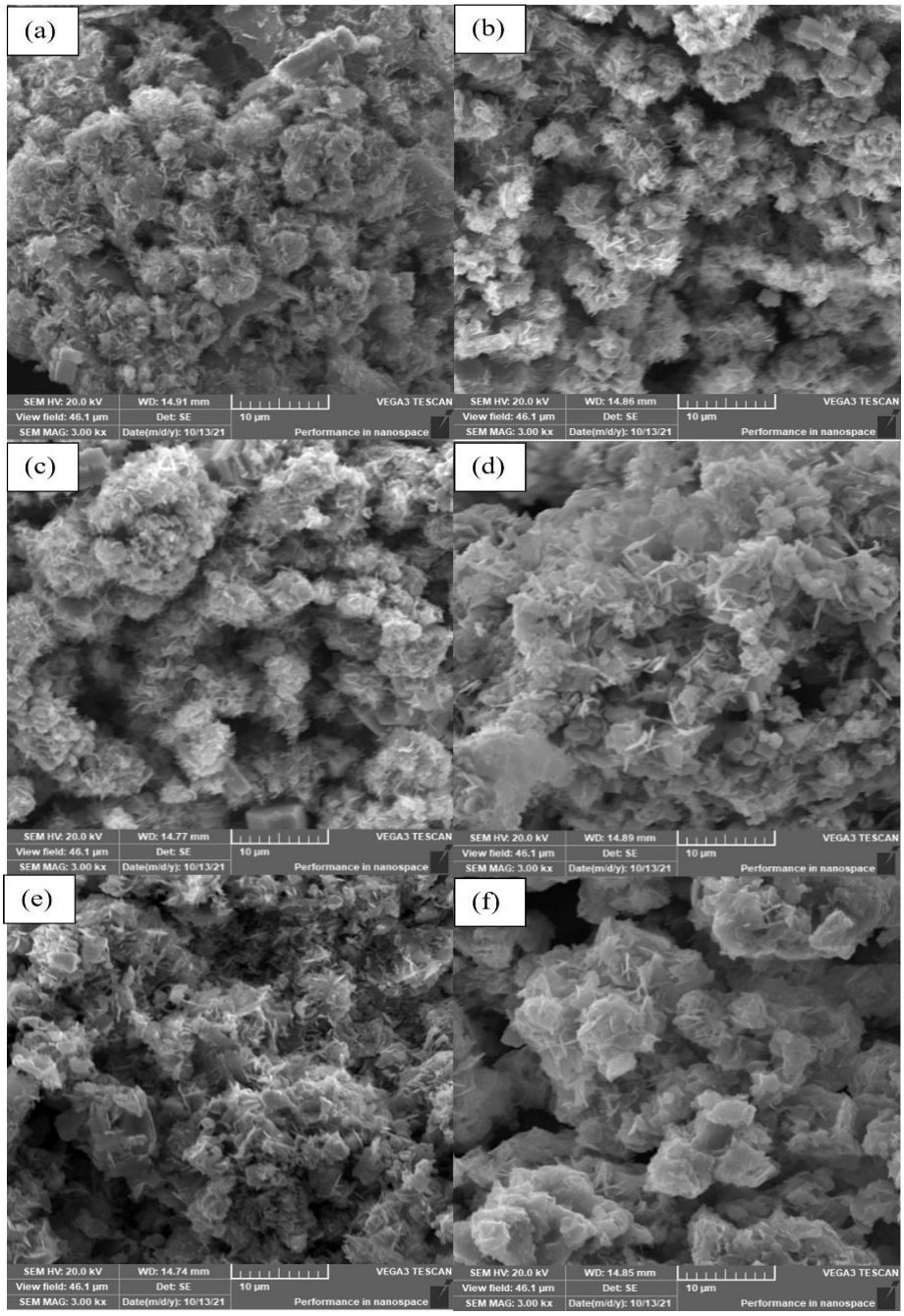

Figure 3: SEM images of (a) undoped ZnO, (b) 10, (c)20, (d) 30, (e) 40 and (f) 50 mol% NiO-doped ZnO at 20,000 x magnification

Further characterization of the elemental composition of NiO-doped ZnO was conducted using EDS chemical mapping analysis for sample 10–50 mol % NiO-doped ZnO as shown in Figure 4. Figure 4 (a) –(e) shows the EDS images of NiO-doped ZnO from 10 to 50 mol % and individual element distribution mapping, respectively. The EDS analysis confirmed that the Ni element is detected in the sample of NiO-doped ZnO. The EDS analysis shows the presence of Ni, Zn and O with no other impurities peak detected in the EDS spectra, confirming the purity of the samples. The images represented elements by red, green and yellow for Zn, O and Ni, respectively. As expected from the mapping analysis, elements Zn, O and Ni showed complete coverage of the image frame, and the Ni element was scattered homogeneously on the ZnO structure. Quantitative analysis of dopant concentrations is also represented in the figures for 10 – 50 mol % NiO-doped ZnO. The peak of Ni incorporated in EDS spectra and the weight percentage of Ni element increased as the concentration of dopant increased for NiO-doped ZnO (10 to 50 mol %) with the value of 0.34 wt% up to 15.78 wt% of Ni element, respectively. Generally, IR spectroscopy is a useful method to study organic compounds based on the specific absorption peaks of their functional groups. The FTIR absorption spectra of the relevant components are shown in Figure 5 in the range of 4000 – 500 cm^{-1} for undoped and doped ZnO samples. The peaks represent the distinctive functional group present in the ZnO-NiO nanoparticles that were produced. The absorption peak from 503 cm^{-1} to 564 cm^{-1} corresponds to the vibration mode of metal-oxygen (Zn-O stretching vibrations) and peak at 1570 cm^{-1} corresponds to the OH bending [22]. The peaks at 2834 cm^{-1} and 3305 cm^{-1} are attributed to hydroxyl compounds' stretching vibration. The broad absorption band in the range of 600–700 cm^{-1} is attributed to the Ni–O stretching vibration mode; the wide absorption band implies that NiO particles are nanocrystals [24]. In addition to the Ni–O vibration, Figure 5 reveals that the broad absorption band centred at 3411 cm^{-1} is attributed to the band O–H stretching vibrations and the weak absorption band near 1688 cm^{-1} is attributable to H–O–H bending vibrations mode due to the adsorption of water in the air during the preparation of the sample which similar findings have been reported by Rezaie et al. [25]. As depicted in Figure 5 (b), all the above-mentioned peaks appeared in the spectrum of the samples with slight shifts that showed the interaction effects between the species.

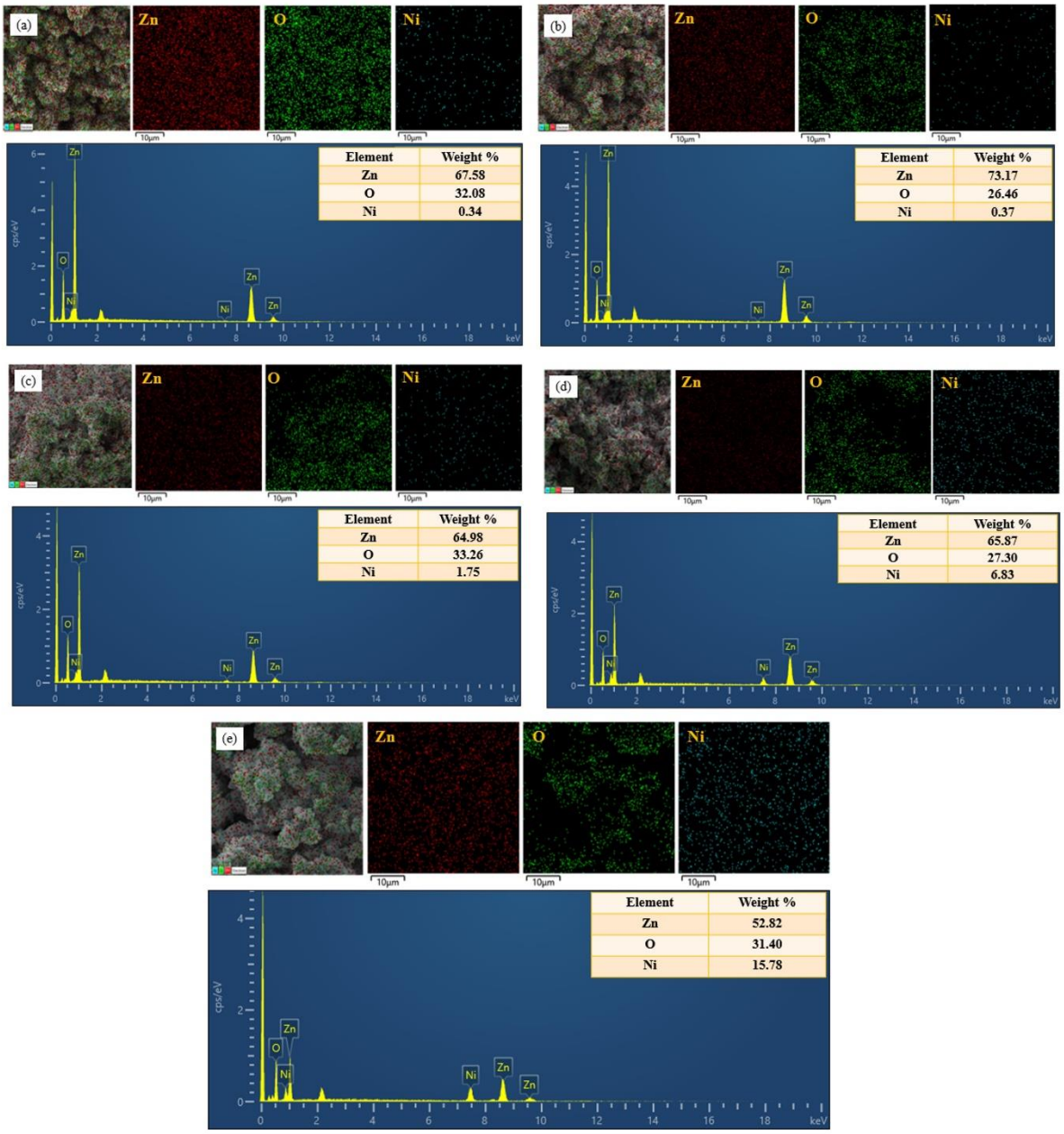

Figure 4: EDS characterization, elemental mapping and spectrum of NiO-doped ZnO prepared by sol gel method: (a) 10, (b) 20, (c) 30, (d) 40 and (e) 50 mol%

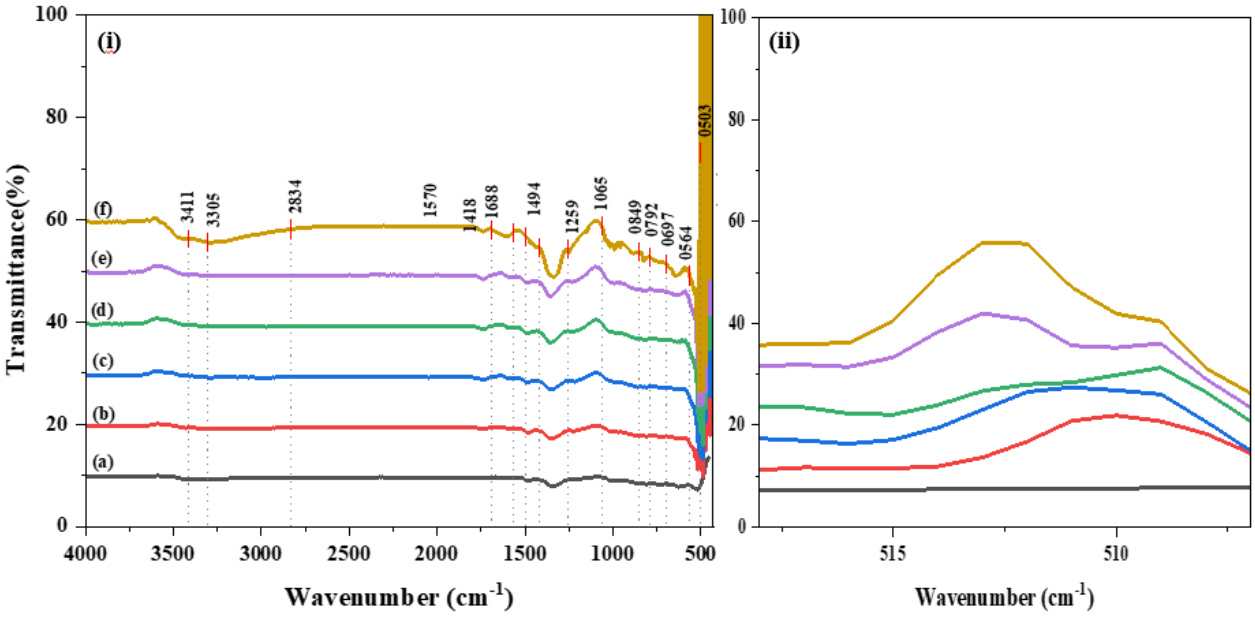

Figure 5: FTIR spectra (i) :(a) undoped ZnO, (b) 10 mol%, (c) 20 mol%, (d) 30 mol%, (e) 40 mol% and (f) 50 mol% NiO-doped ZnO (Range: 4000 – 500 cm^{-1}), (ii): Shift of the absorption peaks by NiO doping (Range: 520 -500 cm^{-1})

CONCLUSION

In conclusion, undoped ZnO and NiO-doped ZnO with various mol % concentrations ranging from 10 to 50 mol% has been successfully prepared via the precipitation method. The variation in concentration results in the different morphological and crystal structures in terms of their crystallite size. The SEM images show the undoped ZnO and NiO-doped ZnO samples mainly consist of flakes-like particles that evenly distributed and well dispersed with sizes ranging from 100 to 500 nm. The EDS mapping analysis has shown the existence of Ni element in the sample, and the slightly (101) peak ZnO shifted from XRD results has proven that the Ni atoms have been doped in the ZnO samples and the estimated crystallite size of 40.6 – 47.6 nm was obtained by the Scherrer equation for the undoped ZnO and NiO-doped ZnO with various mol % concentrations (10 –50 mol%), respectively. Further investigation on the photocatalytic performance of prepared sample of NiO-doped ZnO will be investigated as it may be one of the promising candidates for photocatalysis applications.

ACKNOWLEDGMENTS

The authors gratefully acknowledge the Ministry of Higher Education Malaysia (MOHE) for the financial support under FRGS-RACER grants (600-IRMI/FRGS-RACER 5/3 (041/2019)). We also like to thank Universiti Teknologi MARA (UiTM), Research Management & Innovation Institute (IRMI), and NANO-Electronic Centre for the technical support and characterization measurement.

REFERENCES

[1] E.E. El-Katori, E.A. Kasim, D.A. Ali (2022). *Colloids Surfaces A Physicochemical Engineering Aspect*, **636**, 128153.

[2] A. Di Mauro, M.E. Fragalà, V. Privitera, G. Impellizzeri (2017). *Materials Science in Semiconductor Processing*, **69**, 44

[3] Y. Al-Hadeethi, A. Umar, S.H. Al-Heniti, R. Kumar, S. Kim, X. Zhang, B.M. Raffah (2017). *Ceramics International*, **43**(2), 2418

[4] J. Luo, J., Xia, H. Yang, L. Chen, Z. Wan, F. Han, H.A. Malik, X. Zhu, C. Jia (2018). *Energy & Environmental Science*. **11**(8), 2035

[5] M. Samadi, M. Zirak, A. Naseri, E. Khorashadizade, A.Z. Moshfegh, *Thin Solid Films*, **605**, pp. 2–19 (2016)

[6] A. Boukhari, B. Deghfel, A. Mahroug, R. Amari, N. Selmi, S. Kheawhom, A.A. Mohamad (2022). *Ceramics International*, **47**(12), 17276

[7] U.S. Udayachandran Thampy, A. Mahesh, K.S. Sibi, I.N. Jawahar, V. Biju (2019). *SN Applied Sciences*, **1**, 1478

[8] S.M. Aydoghmish, S.A. Hassanzadeh-Tabrizi, A. Saffar-Teluri (2019) *Ceramics International*, **45**, 14934

[9] F. Aziz, H.M. Abo-Dief, A. Warsi, M.F. Warsi, M. Shahid, T. Ahmad, G.A.M. Mersal, M.M. Ibrahim (2022). *Phys. B Condens. Matter*, **640,** 413858

[10] F. Abbasi, F. Zahedi, F., M.H. Yousefi (2021). *Optics Communications*, **482**, 126565

[11] D. Han, M.J. Currell, G. Cao (2016). *Environmental Pollution*, **218**, 1222

[12] J. Rosowska, J. Kaszewski, B. Witkowski, L. Wachnicki, M. Godlewski (2016). *Acta Physica Polonica A*, **130**(5), 1205

[13] Z. Mirghiasi, F. Bakhtiari, E. Darezereshki, E. Esmaeilzadeh (2014). *Journal of Industrial and Engineering Chemistry*, **20**(1), 113

[14] M. Albert, C. Golla, C. Meier (2021). *Journal of Crystal Growth*, **557**, 126009

[15] S. Iwan, J.L. Zhao, S.T. Tan, X.W. Sun (2018). *Vacuum*, **155**, 408

[16] J. Jiang, L. Zhu, Y. Wu, Y. Zeng, H. He, J. Lin, Z. Ye (2012). *Materials Letters*, **68**, 258

[17] Y. Alajlani, F. Placido, D. Gibson, H.O. Chu, S. Song, L. Porteous, S. Moh (2016). S*urface Coatings Technology*, **290**,16–20

[18] H.S. Al-Salman, M.J. Abdullah (2013). *Journal of Alloys Compounds*, **547**, 132

[19] C. Rojas-Michea, M. Morel, F. Gracia, G. Morell, E. Mosquera (2020). *Surfaces and Interfaces*, **21**, 100700

[20] N.H. Erdogan, T. Kutlu, N. Sedefoglu, H. Kavak (2021). *Journal of Alloys Compounds*, **881**, 160554

[21] M.F. Nsib, S. Saafi, A. Rayes, N. Moussa, A. Houas (2016). *J. Energy Inst*. **89**, 694.

[22] A.A. Nada, H. Selim, M. Bechelany, M. El-Sayed, R. M. Hegazey, E.R. Souaya, M.F. Kotkata (2018). *Mater. Sci. Pol*. **36,** 327.

[23] P. Bindu, S. Thomas (2014). *Journal of Theoretical and Applied Physics*, **8**(4), 123

[24] H. Qiao, Z. Wei, H. Yang, L. Zhu, X. Yan, (2009). *Journal of Nanomaterials*, **2009,** 1

[25] M. Rezaei, A. Nezamzadeh-Ejhieha (2020). *Int. J. Hydrogen Energy*, **45**, 24749